MITSUBISHI ELECTRIC RESEARCH LABORATORIES
https://www.merl.com

Learning Generalizable Pivoting Skills with Object Feature Based State/Action Projections

Zhang, Xiang; Jain, Siddarth; Huang, Baichuan; Tomizuka, Masayoshi; Romeres, Diego

TR2023-048 May 25, 2023

Abstract

The task of pivoting an object with a robotic manipulator is challenging due to the precise application of force required to maintain contact with the object. However, even if the robot is capable of pivoting a particular object, generalizing these skills across different objects presents a more complex challenge. In this paper, we propose a method for generalizing a single-object pivoting skill to other objects by utilizing object visual features. Specifically, we train an encoder to extract the kinematic properties of arbitrary objects from their depth images. Then, we learn projections based on these properties to adjust the state and action space to adapt the single-object pivoting skill to the new pivoting task. The proposed approach is entirely trained in simulation. It requires only one depth image of the object and can zero-shot transfer to real-world objects. We demonstrate robustness to sim-to-real transfer and generalization to multiple objects.

ICRA 2023 Workshop on Effective Representations, Abstractions, and Priors for Robot Learning (RAP4Robots)

Mitsubishi Electric Research Laboratories, Inc.
201 Broadway, Cambridge, Massachusetts 02139

Learning Generalizable Pivoting Skills with Object Feature Based State/Action Projections

Xiang Zhang[1], Siddarth Jain[2], Baichuan Huang[3], Masayoshi Tomizuka[1], and Diego Romeres[2]

***Abstract*— The task of pivoting an object with a robotic manipulator is challenging due to the precise application of force required to maintain contact with the object. However, even if the robot is capable of pivoting a particular object, generalizing these skills across different objects presents a more complex challenge. In this paper, we propose a method for generalizing a single-object pivoting skill to other objects by utilizing object visual features. Specifically, we train an encoder to extract the kinematic properties of arbitrary objects from their depth images. Then, we learn projections based on these properties to adjust the state and action space to adapt the single-object pivoting skill to the new pivoting task. The proposed approach is entirely trained in simulation. It requires only one depth image of the object and can zero-shot transfer to real-world objects. We demonstrate robustness to sim-to-real transfer and generalization to multiple objects.**

I. INTRODUCTION

Table-top manipulation skills like pivoting are required to reorient objects often to create pre-conditions for other manipulation skills. For example, a book on the table may be too large for a robot to grasp, and a peg may lay in the wrong orientation for an insertion task. However, reorienting the book and the peg with a pivoting motion creates the conditions for a successful grasp. Fig. 1(a) depicts the pivoting setup when the object is between two external surfaces, and the robot needs to exploit the interaction with these surfaces to pivot the object. A significant difficulty for pivoting is that the robot must maintain the object-gripper and object-surfaces contacts. Furthermore, multiple objects' different kinematic and inertial properties entail additional complexity like instability, slipping, and rolling properties.

This paper proposes a framework for learning a generalizable robotic skill of pivoting real-world objects from only simulation experience. Specifically, we would like to adapt the pivoting policy on one object to multi-objects based on the object depth image. An overview of our approach is shown in Fig 1(b). We assume that a pivoting policy is available to pivot one specific object, which we call the "unitary" object. Such a policy can be learned either by reinforcement learning or imitation learning. the proposed framework consists of three parts. Then, to extract object kinematic properties from object depth images, we employed supervised learning on a dataset collected in simulation to learn a feature space by predicting the object class and size. Finally, object-specific state and action projections are learned to adapt the unitary policy to a novel object by adjusting the state and action space. These projects are linear transformations obtained from the object features and learned with a policy-gradient based approach. Intuitively, the state projections adjust the states of the new object to make it similar to the unitary object. Accordingly to the new object, the action projections alter policy outputs to improve policy performance. The proposed approach is trained entirely in the simulation and zero-shot transferred to a series of real-world pivoting tasks.

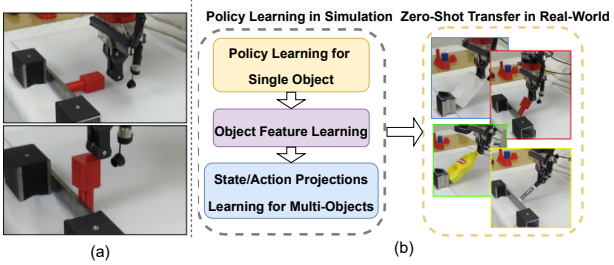

Fig. 1: a) Pivoting task setup. b) policy learning in simulation and zero-shot transfer to real-world

In summary, our work makes following contributions: 1) It introduces a framework to learn generalizable pivoting robotic skills of real-world objects with training only in simulation. 2) It proposes a policy-gradient based approach to learning state/action transformations to achieve generalization to unseen objects. 3) It provides an extensive evaluation of our proposed approach in both simulation and real-world experiments with promising success rates.

II. RELATED WORKS

A. Robot Pivoting Task

A robot pivoting task is a type of manipulation task where a robot is required to rotate an object around a fixed point. Previous approaches can be mainly categorized into two classes: model-based methods and model-free methods. Model-based approaches [1] develop open-loop and feedback control strategies by modeling contact dynamics. However, this approach requires precise modeling of the object contact dynamics. The model-free approaches skip the complex contact dynamics modeling and directly learn a policy to achieve the manipulation task. Specifically, authors of [2] investigated pivoting tasks using RL. However, their pivoting policy is learned on one object during training and can only apply to similar-sized objects, limiting their application.

[1]Mechanical Systems Control Lab, UC Berkeley, Berkeley, CA, USA. {xiang_zhang_98, tomizuka}@berkeley.edu
[2]Mitsubishi Electric Research Laboratories (MERL), Cambridge, MA, USA {sjain,romeres@merl}.com
[3]Department of Computer Science, Rutgers University, Piscataway, NJ, USA. baichuan.huang@rutgers.edu

B. Learning Generalizable Robot Skills

Generalization is a significant concern for robot skill learning because we are interested in robot skills that are robust to environments and task condition changes. However, it is indeed a difficult task since different objects have different geometric shapes, physical properties, and contact dynamics. Researchers have proposed approaches to learn robust skills that work for different task settings or can adapt quickly to new tasks. Domain randomization [3] can be applied for robustness to force the learned policy to extract useful information from the state. Furthermore, Meta RL is applied to quickly adapt to new, unseen tasks based on experience gained from previous tasks. Examples can be found in both gradient-based methods[4] which learns a set of policy parameters that can adapt to new tasks in a few trials and contextual-based methods [5]–[8] which encode the task information into the policy.

Researchers also consider skill generalization as a domain adaptation problem. For different tasks, the state and action space may vary depending on the task settings, such as the robot and object shapes, and it is necessary to analyze how to transfer a learned policy to other tasks. One popular approach is to discover a shared latent space between tasks that is invariant to task settings. Once the skill is learned in the invariant latent space, it can be transferred to different task settings using task-specific mappings [9], [10]. Alternatively, direct mapping on the state or action space can be applied to transfer the skill in the source domain to the test domain [11], [12]. However, in these prior approaches, the state or action space mappings are either obtained manually by analyzing the differences between spaces or by utilizing the point cloud registration algorithm, which relies on prior human knowledge. In contrast, our proposed method automatically discovers the underlying mappings on the state or action space by maximizing the trajectory return, thereby eliminating the need for prior human knowledge.

III. PROBLEM FORMULATION

The pivoting task setting is depicted in Fig 1(a), where a rigid object o is at rest on a flat surface like a table, and it is in the proximity of a second surface, called wall, perpendicular to the table. The object o can be manipulated by any end-effector of a robotic manipulator that can establish a patch contact with the object, like the fingers of a gripper. The goal is to learn a policy, $\pi(\cdot|s)$ where s is the system state, that can utilize the environmental contacts gripper-object, object-table, and object-wall to pivot the object to stand-up.

In this work, we propose a framework to learn the robotic skill of pivoting real-world objects in a structured environment with zero-shot transfer learning from simulation to the real world. The main focus is generalizing the learned pivoting skill to arbitrary unseen objects.

IV. PROPOSED APPROACH

In this section, we introduce our proposed approach to solve the problem described in Section III. The basic idea is that the pivoting operation of different objects might be computed as a transformation of a policy learned on one primary object rather than be learned from scratch every time. We decompose the approach into three main steps. First, a pivoting policy is learned in simulation for an arbitrary object, denominated the *"Unitary"* object. Second, a latent space of object features is learned to represent the shape of objects based on synthetic depth images generated in simulation. Finally, two neural networks are trained to adapt the unitary policy to a novel object by adjusting the state and action space. The overall framework is shown in Fig 2, and the steps are detailed in the following section.

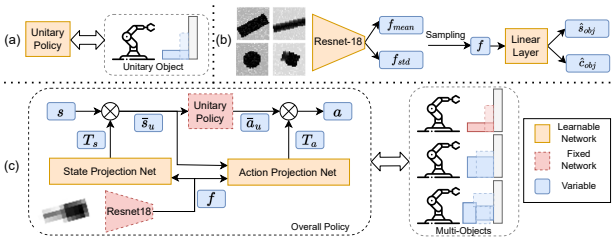

Fig. 2: Three steps of pivoting policy learning in simulation: a) learning pivoting policy on the unitary object. b) object feature learning by predicting object class and size c) state/action projection nets learning on multi-objects pivoting

A. Reinforcement Learning for Pivoting the Unitary Object

The first step in our approach is to acquire a pivoting policy that can manipulate a single arbitrary object, which we refer to as a "unitary" object. To this end, we utilized Reinforcement Learning (RL) to learn a pivoting policy denoted as $\pi(a|s)$, where a is the robot's action that includes the linear velocity of the robot gripper in the X, Y, and Z axes as well as the angular velocity in the pitch direction, and s denotes the state that contains the poses of the gripper and the object, along with the external forces measured by the F/T sensor at the robot wrist. More details of RL training can be found in Appendix I.

B. Representation Learning for Object Features

The objective is to adapt the pivoting unitary policy to work with multiple objects. The kinematic information of the novel object is required to achieve this goal. We rely on representation learning to learn a low-dimensional feature space of the object based on their top-down depth images.

Fig 2(b) shows the proposed network $F(f|\mathcal{I})$ to learn the object features f based on the object depth image $\mathcal{I}$. First, the standard Resnet18 architecture [13] processes the object depth image $\mathcal{I}$ and outputs the mean, and the standard deviation of the object features f_{mean} and f_{std}. Second, similarly to the variational auto-encoder [14], we use the reparametrization trick to sample the object feature f. Finally, another linear layer outputs the predicted object size $\hat{s}_{obj}$ and logits for the object class $\hat{c}_{obj}$. The loss function to train the network is designed as follows:

$$L = L_{shape} + L_{class} + \beta L_{KL} = \|s_{obj} - \hat{s}_{obj}\|^2 + L_{CE}(c_{obj}, \hat{c}_{obj}) + \beta D_{KL}(N(f_{mean}, f_{std}), N(0,1))$$

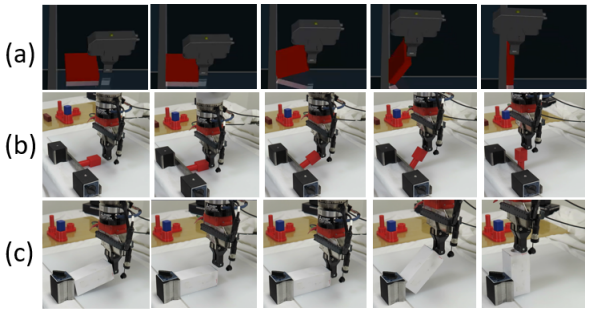

Fig. 3: Snapshots of: a) pivoting the unitary object in simulation b) pivoting a peg in real-world c) recovery behavior.

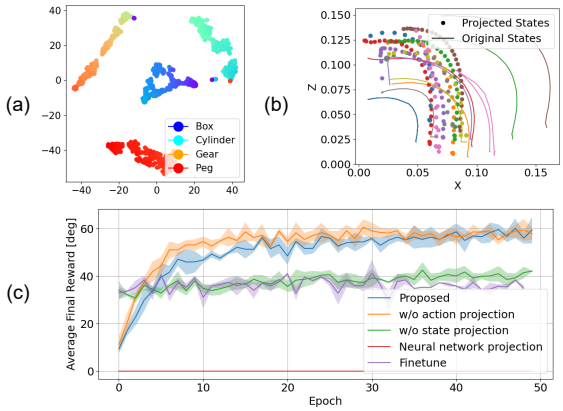

Fig. 4: a) t-SNE visualization of learned object features, color difference within the same class indicates different object size, b) pivoting trajectories before and after projection of different objects, c) learning curves for policy adaption

where L_{CE} is the cross entropy loss and β is a weight on the KL divergence loss. The first two terms of the loss are for supervised learning to predict the object size and class. The KL divergence loss regulates the learned feature space and mitigates over-fitting [14]. In our approach, we rely on the simulated object depth images to train features. Appendix II includes the details of the generated dataset.

C. State and Action Projection Nets

The single object pivoting used in Section IV-A does not generalize to objects with significantly different kinematic properties. However, as shown in Fig 4(b), the trajectories of different objects during pivoting are similar in shape and possibly can be described by trivial transformations in the right space. Inspired by this intuition, we propose learning object-based transformations to adjust the state and action spaces and generalize the unitary policy to novel objects instead of learning from scratch. Specifically, we choose to use linear transformations for simplicity and call these transformations *state* and *action projection nets* as depicted in Fig 2(c). The *State Projection Net*: $T_s = \rho_\phi(f)$ is parameterized by ϕ, and takes as input the feature of the object f to output a diagonal matrix T_s of state dimensions. The output is used as a linear operator to project the object state, s, to a space similar to the unitary state $\bar{s}_u$: $\bar{s}_u = T_s s$. The projected state $\bar{s}_u$ is fed into the unitary policy $\bar{a}_u = \pi^u_\theta(\bar{a}_u|\bar{s}_u)$ to generate the pivoting action. However, $\bar{a}_u$ needs to be transformed to work into the original object. For this reason, we train the *Action Transformation Net*: $T_a = \rho_\psi(f, \bar{s}_u)$, that given f, s_u outputs a diagonal matrix T_a of action dimensions. That is used to compute the pivoting actions: $a = T_a \bar{a}_u$. The overall action inference process can be summarized as:

$$a = T_a \bar{a}_u = T_a \pi^u_\theta(\bar{a}_u|\bar{s}_u) = T_a \pi^u_\theta(\bar{a}_u|T_s s) \tag{1}$$

Thus, the overall generalizable pivoting policy consists of: the unitary policy, the object feature extraction network, and the state/action projection nets. The former two are already trained, and the weights are frozen. Only the state/action projection nets need to be trained to adapt the pivoting policy to different objects. In particular, we use a policy gradient approach to learn the state/action projection nets to maximize the trajectory return of pivoting different objects. Suppose we collected a pivoting trajectory $\tau = (s_1, a_1, T_s, T_a, f, r_1, \ldots, s_T, a_T, T_s, T_a, f, r_T)$ of an object with feature f, the advantage functions of the state/action transformation nets are, respectively:

$$\hat{A}_s = \frac{1}{T}\sum_{i=0}^{T} \gamma^i r_i; \hat{A}_{at} = \sum_{i=t}^{T} \gamma^i r_i \tag{2}$$

where r_i is the reward at time i and γ is the discount factor. Then both state and action projection nets can be learned by maximizing these two objectives. In our approach, we choose to use PPO [15] to update two projection nets by RL. More training details are summarized in Appendix III.

V. EXPERIMENTS

A. Simulation: Training and Validation Experiments

RL for Pivoting Unitary Object: We first test the single object pivoting policy in simulation. Fig 3(a) depicts a sequence of snapshots of pivoting the unitary object in simulation after training the policy. The gripper first pushes the object towards the wall to establish contact between the object and the wall. Then, the robot moves upwards to rotate the object against the wall. Finally, the object is flipped up and standing on the table.

Representation Learning of Object Features: We then evaluated the encoding neural network described in Section IV-B using the t-SNE method [16]. As shown in Fig 4(a), object features are clustered into four groups in the learned feature space, representing four object classes. In addition, within each class, this feature space can distinguish the size information of different objects, which shows the learned feature space can be utilized for downstream tasks.

State/Action Projection Nets Training: Once the unitary policy and the object features are learned, the *State/Action Projection Nets* are trained on 40 randomly-sized objects, 10 objects for each class c_{obj}. Since the elements of quaternions in the state are coupled and will be distorted by the transformation, we only apply the same projection to both the

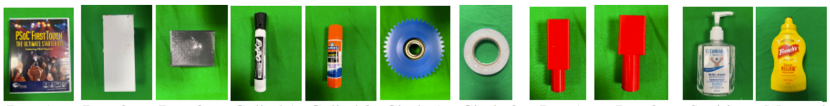

	Box 1	Box 2	Box 3	Cylind.1	Cylind.2	Circle 1	Circle 2	Peg 1	Peg 2	Sanitizer	Mustard
April-Tag	10/10	10/10	10/10	9/10	9/10	10/10	10/10	9/10	10/10	10/10	10/10
Vision tracking	10/10	7/10	10/10	10/10	5/10	10/10	10/10	10/10	10/10	10/10	7/10

Fig. 5: Test objects and success rates for the two vision systems

object and gripper positions for the state projection net, that is $T_s \in \mathbb{R}^{3\times3}$ and $T_a \in \mathbb{R}^{4\times4}$ remains unchanged.

Multi-objects generalization performances: The proposed approach is evaluated in simulation and compared against three ablation studies and two baselines:

1) *NN projections*: train two neural networks $\bar{s}_u = \rho_s(f, s)$, $a = \rho_a(f, \bar{s}_u)$ to replace the linear transformations in the state/action projection nets;
2) *w/o state*: our approach without state projection net;
3) *w/o action*: our approach without action projection net;
4) *Finetune*: the unitary policy is fine tuned using PPO without state and action projection nets;
5) *Pearl*: train one s.o.t.a. Meta-RL approach, Pearl [8].

As depicted in Fig 4(c), the proposed approach and the ablation *w/o action* outperform all the other approaches. The *NN projections* does not adapt the unitary policy to multi-objects, possibly because it cannot use the structure of the linear transformation and might require much more data to learn the task. We also notice that the state projection net helps the most for adaption and converges faster than the proposed method. The reason is that the proposed method's action projection is not perfect initially and slows down the training. However, as shown in Table I, the proposed method achieves a higher success rate than all the baselines, which indicates the action projection helps to adjust policy according to the object feature. In our experiments, Pearl can approach the objects but cannot learn to pivot for multiple objects. We conclude that the objects are too different, making it difficult for Pearl to learn a policy for all objects from scratch. Since the objects in the simulation are randomly generated, some objects have small surfaces to stand on compared to their sizes, which makes them challenging to pivot, and our approach fails.

Ours	w/o action	w/o state	Finetune	NN	Pearl
30/40	27/40	19/40	15/40	0/40	0/40

TABLE I: Average success rates on 40 objects in the training environment over 3 random runs

We further analyze the effect of the state projection net by plotting the pivoting trajectories of different objects before and after the projection in the two most representative axis X, Z. As depicted in Fig 4(b), even though the original trajectories are very diverse (solid lines), the projection net brings the pivoting trajectories together, enabling the unitary policy to adapt to new objects.

B. Real-World Experiments

The proposed approach is evaluated with zero-shot transfer learning over all objects. An experiment is deemed successful when an object reaches a stable stand-up position, and the success rates are shown in Fig 5. We start the analysis considering the April-Tag system to estimate the state. Even though the shapes and sizes of the objects are very different, i.e., $l_x = [6, 18.5], l_y = [1, 15], l_z = [1, 5][cm]$. our approach achieves 100% success rate on almost all the objects, demonstrating direct sim-to-real transfer capability and generalization to multiple objects. The failure cases happen all in objects with a cylindrical base, i.e., Cylinder 1,2 and Peg 2, because their shape is prone to a rolling behaviour and have a smaller base to stand on. However, the policy is robust to these difficulties in most of the cases and failed only once. Successful pivoting experiments are visualized with a sequence of snapshots in Fig 3(b)-(c).

Next, we test the generalization to two out-of-distribution objects: "sanitizer" and the "mustard bottle". The shapes of these two objects are complex, non-convex and with irregular contact surfaces that are not flat. Moreover, no similarly shaped object is considered in training. However, our approach succeeds on these two objects with 100% success rate and demonstrates generalizability properties.

Finally, we evaluate the performance when using the vision tracking system that returns more noisy state estimations. As shown in Fig 5, we still achieves 100% success rates for most objects. The failure cases are due to excessive noise in the state: in Box 2 because the object has no texture, in Cylinder 2 because the object is very small, and for the Mustard bottle the tracking gets lost when close to the goal.

VI. CONCLUSIONS

We propose a framework to learn robotic skills for pivoting real-world objects. The method is trained only in simulation, requiring only one depth image of the manipulated object to transfer to real-world tasks. Moreover, the same policy generalizes to pivot multiple real-world objects. The main idea is based on learning a robust RL policy for a "unitary" object and then learning two projection networks that adapt the states and actions fed into/outputted by such a policy. An object feature space is learned from top-down view depth images of the objects to encode the kinematic properties such as size and shape. The real-world experiments show a successful zero-shot transferring for sim2real gap and generalization to multiple objects.

REFERENCES

[1] Y. Shirai, D. K. Jha, A. U. Raghunathan, and D. Romeres, "Robust pivoting: Exploiting frictional stability using bilevel optimization," in *2022 International Conference on Robotics and Automation (ICRA)*, 2022, pp. 992–998.

[2] W. Zhou and D. Held, "Learning to grasp the ungraspable with emergent extrinsic dexterity," in *ICRA 2022 Workshop: Reinforcement Learning for Contact-Rich Manipulation*, 2022. [Online]. Available: https://openreview.net/forum?id=Zrp4wpa9lqh

[3] M. Laskin, K. Lee, A. Stooke, L. Pinto, P. Abbeel, and A. Srinivas, "Reinforcement learning with augmented data," *Advances in neural information processing systems*, vol. 33, pp. 19 884–19 895, 2020.

[4] C. Finn, P. Abbeel, and S. Levine, "Model-agnostic meta-learning for fast adaptation of deep networks," in *International conference on machine learning*. PMLR, 2017, pp. 1126–1135.

[5] T. Z. Zhao, J. Luo, O. Sushkov, R. Pevceviciute, N. Heess, J. Scholz, S. Schaal, and S. Levine, "Offline meta-reinforcement learning for industrial insertion," in *2022 International Conference on Robotics and Automation (ICRA)*. IEEE, 2022, pp. 6386–6393.

[6] K. Hausman, J. T. Springenberg, Z. Wang, N. Heess, and M. Riedmiller, "Learning an embedding space for transferable robot skills," in *International Conference on Learning Representations*, 2018.

[7] T. Li, N. Lambert, R. Calandra, F. Meier, and A. Rai, "Learning generalizable locomotion skills with hierarchical reinforcement learning," in *2020 IEEE International Conference on Robotics and Automation (ICRA)*. IEEE, 2020, pp. 413–419.

[8] K. Rakelly, A. Zhou, C. Finn, S. Levine, and D. Quillen, "Efficient off-policy meta-reinforcement learning via probabilistic context variables," in *International conference on machine learning*. PMLR, 2019, pp. 5331–5340.

[9] Z.-H. Yin, L. Sun, H. Ma, M. Tomizuka, and W.-J. Li, "Cross domain robot imitation with invariant representation," in *2022 International Conference on Robotics and Automation (ICRA)*. IEEE, 2022, pp. 455–461.

[10] K. Kim, Y. Gu, J. Song, S. Zhao, and S. Ermon, "Domain adaptive imitation learning," in *International Conference on Machine Learning*. PMLR, 2020, pp. 5286–5295.

[11] M. E. Taylor, P. Stone, and Y. Liu, "Transfer learning via inter-task mappings for temporal difference learning." *Journal of Machine Learning Research*, vol. 8, no. 9, 2007.

[12] T. Tang, C. Liu, W. Chen, and M. Tomizuka, "Robotic manipulation of deformable objects by tangent space mapping and non-rigid registration," in *2016 IEEE/RSJ International Conference on Intelligent Robots and Systems (IROS)*, 2016, pp. 2689–2696.

[13] K. He, X. Zhang, S. Ren, and J. Sun, "Deep residual learning for image recognition," in *Proceedings of the IEEE conference on computer vision and pattern recognition*, 2016, pp. 770–778.

[14] D. P. Kingma and M. Welling, "Auto-encoding variational bayes," *arXiv preprint arXiv:1312.6114*, 2013.

[15] J. Schulman, F. Wolski, P. Dhariwal, A. Radford, and O. Klimov, "Proximal policy optimization algorithms," *arXiv preprint arXiv:1707.06347*, 2017.

[16] L. Van der Maaten and G. Hinton, "Visualizing data using t-sne." *Journal of machine learning research*, vol. 9, no. 11, 2008.

[17] E. Todorov, T. Erez, and Y. Tassa, "Mujoco: A physics engine for model-based control," in *2012 IEEE/RSJ Int. Conf. on Intelligent Robots and Syst.* IEEE, 2012, pp. 5026–5033.

[18] T. Haarnoja, A. Zhou, K. Hartikainen, G. Tucker, S. Ha, J. Tan, V. Kumar, H. Zhu, A. Gupta, P. Abbeel *et al.*, "Soft actor-critic algorithms and applications," *arXiv preprint arXiv:1812.05905*, 2018.

[19] Rail-Berkeley, "Rail-berkeley/rlkit: Collection of reinforcement learning algorithms." [Online]. Available: https://github.com/rail-berkeley/rlkit

[20] E. Olson, "Apriltag: A robust and flexible visual fiducial system," in *2011 IEEE international conference on robotics and automation*. IEEE, 2011, pp. 3400–3407.

[21] C. Mayer, M. Danelljan, G. Bhat, M. Paul, D. P. Paudel, F. Yu, and L. Van Gool, "Transforming model prediction for tracking," in *Proceedings of the IEEE/CVF Conference on Computer Vision and Pattern Recognition*, 2022, pp. 8731–8740.

[22] J. Revaud, P. Weinzaepfel, C. De Souza, N. Pion, G. Csurka, Y. Cabon, and M. Humenberger, "R2d2: repeatable and reliable detector and descriptor," *arXiv preprint arXiv:1906.06195*, 2019.

[23] B. Huang, J. Yu, and S. Jain, "EARL: Eye-on-hand reinforcement learner for dynamic grasping with active pose estimation," 2023.

[24] B. Wen and K. Bekris, "Bundletrack: 6d pose tracking for novel objects without instance or category-level 3d models," in *2021 IEEE/RSJ International Conference on Intelligent Robots and Systems (IROS)*. IEEE, 2021, pp. 8067–8074.

APPENDIX

APPENDIX I
DETAILED REINFORCEMENT LEARNING SETUP FOR UNITARY OBJECT PIVOTING

The simulation environment. The unitary pivoting policy $\pi^u_\theta(a|s)$ parameterized by θ is learned in a Mujoco [17] simulation environment, as shown in Fig. 6(a). The simulation includes the robot gripper and the unitary object, which is a $9 \times 9 \times 3$ cm^3 box. The dimensions are arbitrarily chosen, and they don't affect the algorithm. Moreover, a rigid wall is placed at what we consider the world frame origin to act as an external surface.

The details to train $\pi^u_\theta(a|s)$ are as follows:

The state space is defined by three components: object pose s_o, gripper pose s_g, and the external forces measured by the F/T sensor at the wrist of the robotic manipulator, right above the gripper, s_F. The object and gripper pose include the cartesian position (X, Y, Z axes) and orientation in quaternion, $s_o, s_g \in \mathbb{R}^7$ while s_F contains the forces measured along the X, Y, and Z axes, $s_F \in \mathbb{R}^3$. Thus, the state $s := [s_o, s_g, s_F] \in \mathbb{R}^{17}$. The maximum forces applied by the robot in the simulation are $\pm 10N$ in each axes, and s_F is normalized to $\pm 1N$.

The action space is defined by the linear velocity of the robot gripper in X, Y, and Z axes as well as the angular velocity in the pitch direction, $a = [a_x, a_y, a_z, a_\rho] \in \mathbb{R}^4$. The actions are limited by a moving threshold set to $25\ mm$. If the gripper moves more than this limit during training, the robot stops and proceeds to the next action.

The reward function is the distance between the current object rotation matrix R and the goal rotation matrix R^{goal} which is defined as:

$$r = \frac{\pi}{2} - d, \text{ with } d = \arccos\left(0.5(\text{Tr}(R^{goal}R^T) - 1)\right) \quad (3)$$

where $Tr(\cdot)$ indicates the trace of a matrix. $\frac{\pi}{2}$ is added to the reward to make the initial reward close to 0. This reward encourages the robot to pivot the object to the goal orientation R^{goal}, which is set as the orientation when the object is perpendicular to the ground.

Domain randomization is employed to improve the robustness of the pivoting policy with three kinds of noises:

1) Uncertainty of the wall position. The origin of the world frame is set at the wall, and we assume the exact position of the wall is unknown. Since the positions of the object and gripper are measured w.r.t the wall, we model this uncertainty by adding a zero-mean Gaussian noise with an std of 2 cm to the object and the gripper positions.

2) Force measurement noise. To model the noise of the F/T sensor measurements, a zero-mean Gaussian noise with an std of $0.5\ N$ is added to the measured force in the simulation.

3) Initial pose distribution. During the training, we randomized the initial pose of the object. Specifically, the object

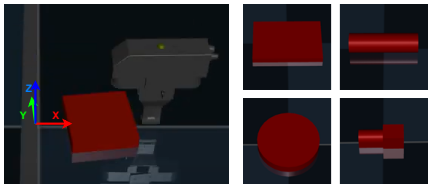

Fig. 6: Simulation in Mujoco: a) training on the unitary object, b) four classes of objects (box, circle, cylinder, peg)

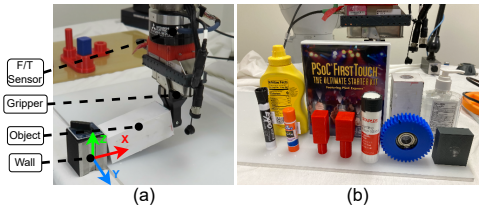

Fig. 7: a) Real-world setup. b) Objects in the real world.

is placed with an offset to the wall and is oriented by a random angle. The initial offset Δ_x is sampled uniformly from range $[0, 5\ cm]$. The initial rotation angle limit is defined as $\pm \arctan(\Delta_x/4.5)$, and the initial rotation angle is sampled from this range to avoid an unfeasible initial pose.

Training hyperparameters: The pivoting policy is trained with the SAC [18] algorithm using the implementation from RLkit [19]. The policy and Q-function networks are parameterized as two-layer Relu networks with 128 and 256 units, respectively. The batch size is 1024, and learning rates are $5e-3$ for the Q-function and $3e-4$ for the policy.

Appendix II
Depth Image Dataset Generation

We first build a dataset of depth images in simulation to learn such a feature space. As depicted in Fig 6(b), we generated the dataset from four object classes c_{obj}: rectangular box, circle, cylinder, and peg. For each class, 100 randomly sized objects are generated. The generated dataset is composed as $\mathcal{D} := \{\mathcal{I}_i, c_{obj,i}, s_{obj,i}\}_i^{400}$ where $\mathcal{I}_i$ are the depth images of each object and $s_{obj,i} = [l_x, l_y, l_z]$ are the sizes, recorded as labels. Then, $\mathcal{D}$ is augmented ten times to 4000 data points by applying random translations, rotations, and Gaussian noise to each original data point.

Appendix III
Learning Projection Networks with PPO

In this paper, we apply a simpler version of PPO [15] to update both state and action projection nets. Given two advantage functions pre-mentioned in 2, the objective function for state and action projection nets are:

$$L_s(f, T_s, \phi, \phi_{old}) = \min\left(\frac{\rho_\phi(f)}{\rho_{\phi_{old}}(f)}, \text{clip}\left(\frac{\rho_\phi(f)}{\rho_{\phi_{old}}(f)}, 1+\epsilon_s, 1-\epsilon_s\right)\right) A_s \tag{4}$$

$$L_a(f, s_u, T_a, \psi, \psi_{old}) = \min\left(\frac{\rho_\psi(f, s_u)}{\rho_{\psi_{old}}(f, s_u)}, \text{clip}\left(\frac{\rho_\psi(f, s_u)}{\rho_{\psi_{old}}(f, s_u)}, 1+\epsilon_a, 1-\epsilon_a\right)\right) A_a \tag{5}$$

where $\frac{\rho_1(\cdot)}{\rho_2(\cdot)}$ is the ratio of likelihood of two projections and ϵ_s, ϵ_a are clipping factors for update. The weights of the two projection nets are updated by:

$$\phi_{k+1} = \underset{\phi}{\text{argmax}} \underset{(f,T_s)\sim\pi_{\phi_k}}{\mathbb{E}} L_s(f, T_s, \phi, \phi_k) \tag{6}$$

$$\psi_{k+1} = \underset{\psi}{\text{argmax}} \underset{(f,s_u,T_s)\sim\pi_{\psi_k}}{\mathbb{E}} L_a(f, s_u, T_a, \psi, \psi_k) \tag{7}$$

Essentially, we maximize the likelihood of state or action transformations with higher reward-to-go. The details of our proposed approach are summarised in Algorithm 1.

Algorithm 1: Learning state and action projections

```
Initialize state and action projection nets
  ρ_φ(f), ρ_ψ(f, s_u) with random weights φ, ψ
Initialize the unitary policy π^u_θ(ā_u|s̄_u) and feature
  extraction network F(f|I) with pretrained weights.
for i = 0, 1, 2, ... until convergence do
    for iteration k = 1 to K do
        Randomly sample an object o_k with image I_k
        Infer the object feature f_k ~ F(f|I_k)
        Infer actions using (1) to collect a trajectory
    end
    Calculate advantages for state and action
      transformations using (2)
    for iteration m = 1 to M do
        Update State/Action Projection Nets (6),(7)
    end
end
```

Appendix IV
Real-World Experimental Setups

Real Robot Setup and Vision Feedback: We use a 6DoF Mitsubishi Assista RV-5AS-D collaborative robot arm with a WSG32 gripper as shown in Fig. 7(a). The robot is controlled in impedance control mode with stiffness set to 12 N/mm. The external forces are measured by wrist mounted F/T sensor. For state estimation, we compare two systems to obtain the object pose from an RGB-D camera (Intel Realsense D435). The first system uses April-tags [20] on the objects for tracking. This system provides high-accuracy state information but needs the tag's placement. The second system comprises vision-based 6D pose estimation consisting of a mask and deep feature extraction [21], [22] pipeline with pose tracking. To accomplish fast tracking of novel objects in motion using RGB-D images, we introduce several augmentations to enhance the pose tracking [23] based on the BundleTrack [24]. The method does not require CAD models, and because of sensor noise, the state estimation can be noisier. We test pivoting manipulation with both systems to evaluate the robustness of our proposed approach.

Object Dataset: Fig 7(b) shows the objects we used for the real-world experiments. We considered nine objects which can be categorized into four object classes in the

simulation to test the sim-to-real transfer performance of the proposed approach. Furthermore, we test the generalizability on two irregularly shaped objects (sanitizer and mustard bottle). Please note that none of these objects was seen during the simulation and the same hold for depth images of the real objects taken by the camera and used to infer object features.